# Exploring chiral rotation in $A \approx 60$ nuclei: Role of residual interactions*

G. L. Ding (丁赣龙)[1#] R. Dong (董荣)[1#] H. Y. Liu (刘虹余)[1] J. Peng (彭婧)[1†] Q. B. Chen (陈启博)[2‡]

[1]School of Physics and Astronomy, Beijing Normal University, Beijing 100875, China
[2]Department of Physics, East China Normal University, Shanghai 200241, China

**Abstract:** To explore the possible existence of nuclear chirality in the $A \approx 60$ mass region, we study the doublet bands built on the configuration $\pi f_{7/2}^{-1} \otimes \nu g_{9/2}^{1}$ using the particle rotor model (PRM) with residual proton-neutron interactions $V_{pn}$ for cobalt isotopes. The energy spectra $E(I)$, energy difference between the doublet bands $\Delta E(I)$, electromagnetic transition probabilities $B(M1)$ and $B(E2)$, and the energy staggering $S(I)$ of the doublet bands are calculated by varying the deformation parameters $\beta$ and $\gamma$ and moment of inertia $\mathscr{J}$. The PRM calculations show that the parameters for the ideal chirality of the configuration $\pi f_{7/2}^{-1} \otimes \nu g_{9/2}^{1}$ are $\beta = 0.25$, $\gamma = 34°$, and $\mathscr{J} = 10\,\hbar^2/\mathrm{MeV}$. Subsequently, PRM calculations adopting these parameters show that $\Delta E(I)$ and $S(I)$ are sensitive to the residual proton-neutron interactions $V_{pn}$. A weaker $V_{pn}$ is more conducive to the existence of nuclear chirality. Finally, the evolution of the chirality with spin $I$ is illustrated using the probability of the total angular momentum along the principal axes ($K$ distribution) and the orientation with respect to the intrinsic frame $\mathscr{P}(\theta,\varphi)$.

**Keywords:** chiral rotation, $A$~60, residual proton-neutron interactions

**DOI:** 10.1088/1674-1137/adc3fd **CSTR:** 32044.14.ChinesePhysicsC.49074101

## I. INTRODUCTION

Nuclear chirality is an exotic phenomenon of spontaneous symmetry breaking, which exists in rapidly rotating nuclei with a triaxial shape and high-$j$ valence particle(s) and hole(s) [1]. In the intrinsic frame of such a system, the angular momenta of valence particle(s) and valence hole(s) are aligned along the short and long axes, respectively, and the angular momentum of the core is aligned with the intermediate axis, which can have the largest moment of inertia to maintain the lowest energy of the system. This topology forms left- and right-handed systems (transformed into each other by the chiral operator $\chi = \mathscr{T}\mathscr{R}(\pi)$) and results in spontaneous chiral symmetry breaking in the intrinsic frame. In the laboratory frame, the broken chiral symmetry would be restored and result in pairs of $\Delta I = 1$ rotational bands called chiral doublet bands, with the same parity and near-degeneracy in energy owing to the effect of quantum tunneling. Since chirality in nuclei was predicted by Frauendorf and Meng in 1997, chiral doublet bands have attracted considerable interest in both theoretical and experimental aspects.

Theoretically, various approaches have been applied to describe chiral doublet bands. For example, the particle rotor model (PRM) [1−16] and its approximation solution based on the time-dependent variation principle [17−19], the titled axis cranking (TAC) approach [20−24], the interacting boson-fermion-fermion model (IBFFM) [25−27], the TAC plus random phase approximation (RPA) [28, 29], the TAC plus collective Hamiltonian method [30−32], the angular momentum projection (AMP) method [33−38], and the time dependent covariant density functional theory [24, 39]. Among them, the PRM describes a system in the laboratory reference frame and provides a good quantum number for the total angular momentum. The energy splitting (band splitting) and quantum tunneling between the doublet bands (the tunneling between different quantum states) can be explained successfully.

Experimentally, more than 60 chiral doublet bands have been observed in many nuclei in a few mass regions of the nuclear chart. For more details, see reviews [40−55] and the references therein. All of the observations of chiral doublet bands have focused on the $A \geqslant 80$ mass regions; therefore, finding candidate chiral doublet bands in lighter mass regions is naturally an exciting and challenging task.

Thus far, the possibility of chiral doublet bands of Co

Received 13 February 2025; Accepted 19 March 2025; Published online 20 March 2025

* Supported by the National Key R&D Program of China (2024YFE0109803) and the National Natural Science Foundation of China (12205103). This research was supported by the Super Computing Center of Beijing Normal University

† E-mail: jpeng@bnu.edu.cn

‡ E-mail: qbchen@phy.ecnu.edu.cn

# These authors contributed equally as the first authors

isopotes [56] and $^{60}$Ni [12] in the $A \approx 60$ mass region has been investigated using the covariant density functional theory (CDFT) and PRM. The high-$j$ particle-hole configuration $\pi f_{7/2}^{-1} \otimes \nu \left[ g_{9/2}^{1} (fp)^{n} \right]$ is suitable for establishing chiral doublet bands, and the basic microscopic inputs for the PRM have been obtained from CDFT calculations in Ref. [56].

To further explore the evidence of the existence of chiral doublet bands in the $A \approx 60$ mass region, in this study, we systematically investigate the configuration $\pi f_{7/2}^{-1} \otimes \nu g_{9/2}^{1}$ using a quantal triaxial PRM with one-particle-one-hole coupled to a triaxial core. Here, the $(fp)$ shell is neglected owing to its low contribution to the angular momentum of valence nucleons. In addition, the residual proton-neutron interaction is considered in the PRM and applied to chiral doublet bands. This interaction is generally considered as the residual force (between valence nucleons) not accounted for by the mean field in which nucleons move and has some effects on the energy staggering in the bands [57]. The effect of such an interaction on nuclear chirality has rarely been investigated.

The paper is organized as follows. The PRM with the residual interaction is introduced in Sec. II. The numerical details are presented in Sec. III. The obtained energy spectra, electromagnetic transition probabilities $B(M1)$ and $B(E2)$, energy splitting $\Delta E$, energy staggering $S(I)$, analysis of angular momentum geometry based on the probability of the total angular momentum along the principal axes ($K$ distribution), and orientation with respective to the intrinsic frame $\mathscr{P}(\theta,\varphi)$ are presented and discussed in detail in Sec. IV. Finally, a summary is given in Sec. V.

## II. THEORETICAL FRAMEWORK

### A. Particle rotor model with residual proton-neutron interaction

As a quantum model consisting of the collective rotation and intrinsic single-particle motions, the PRM [58, 59] has been extensively used to investigate nuclear chirality. In Refs. [1–4, 60], the PRM was applied to discuss the structure of doublet bands with a one-particle-one-hole configuration. With the inclusion of the residual interaction between the valence proton and neutron, the Hamiltonian of the PRM can be expressed as

$$\hat{H}_{\rm PRM} = \hat{H}_{\rm coll} + \hat{H}_{\rm intr} + V_{pn}. \tag{1}$$

Here, $\hat{H}_{\rm coll}$ represents Hamiltonian of the collective rotor:

$$\hat{H}_{\rm coll} = \sum_{k=1}^{3} \frac{\hat{R}_k^2}{2\mathscr{J}_k} = \sum_{k=1}^{3} \frac{\left(\hat{I}_k - \hat{J}_k\right)^2}{2\mathscr{J}_k}, \tag{2}$$

where the indices $k = 1,2,3$ refer to the three principle axes of the body-fixed frame, $\hat{R}_k$, $\hat{I}_k$, and $\hat{J}_k$ denote the angular momentum operators for the core, total nucleus, and valence nucleons, respectively. The moments of inertia for irrotational flow are adopted, *i.e.*, $\mathscr{J}_k = \mathscr{J} \sin^2(\gamma - 2\pi k/3)$, where $\mathscr{J}$ depends on the mass parameter $A$ and quadrupole deformation $\beta$ [61]. In this study, $\mathscr{J}$ is used as an input parameter in the program.

$\hat{H}_{\rm intr}$ describes the intrinsic Hamiltonian of a single valence nucleon in a high-$j$ shell,

$$\hat{H}_{\rm intr} = \pm \frac{1}{2} C \left\{ \cos\gamma \left( \hat{j}_3^2 - \frac{j(j+1)}{3} \right) + \frac{\sin\gamma}{2\sqrt{3}} \left( \hat{j}_+^2 + \hat{j}_-^2 \right) \right\}, \tag{3}$$

where the plus sign refers to a particle and the minus to a hole. The angle $\gamma$ is the triaxial deformation parameter, and the coupling parameter $C$ is

$$C = \left( \frac{123}{8} \sqrt{\frac{5}{\pi}} \right) \frac{2N+3}{j(j+1)} A^{-1/3} \beta \,\text{MeV}, \tag{4}$$

which is proportional to the quadrupole deformation $\beta$ [62].

The general form of the residual proton-neutron interaction is [63]

$$\begin{aligned} V_{pn} = V(r) \big[ & u_0 + u_1 \boldsymbol{\sigma}_p \cdot \boldsymbol{\sigma}_n + u_2 P_{\rm M} + u_3 P_{\rm M} \boldsymbol{\sigma}_p \cdot \boldsymbol{\sigma}_n \\ & + V_{\rm T} S_{12} + V_{\rm TM} P_{\rm M} S_{12} \\ & + V_{\rm E}^{\rm LS} L \cdot S + V_{\rm O}^{\rm LS} P_{\rm M} L \cdot S \big], \end{aligned} \tag{5}$$

where each line respectively represents the central, tensor, and spin-orbit forces. The radial dependence $V(r)$ takes the Gaussian form

$$V(r) = \exp\left(-r^2/r_0^2\right), \tag{6}$$

owing to the short-range nuclear force. For a zero-range force and the Gaussian radial shape, $V_{pn}$ can be simplified in the following form [64]:

$$V_{pn} = \sqrt{8\pi^3} (\hbar/m\omega)^{3/2} \delta\left(\boldsymbol{r}_p - \boldsymbol{r}_n\right) \left(u_0 + u_1 \boldsymbol{\sigma}_p \cdot \boldsymbol{\sigma}_n\right). \tag{7}$$

The strength parameters $u_0$ and $u_1$ are used as input parameters in this work.

### B. Basis

When discussing the nuclear phenomena using the PRM, the total wave function of the PRM Hamiltonian is often expanded into a strong coupling basis, which considers the strong interaction between the intrinsic motion

of valence nucleons and the collective motion of the nucleus. Therefore, the total wave function can be expressed as [12]

$$|IM\rangle = \sum_{K\phi} C_{K\phi}|IMK\phi\rangle, \tag{8}$$

with

$$|IMK\phi\rangle = \frac{1}{\sqrt{2\left(1+\delta_{K0}\delta_{\phi,\bar{\phi}}\right)}} \times \left(|IMK\rangle|\phi\rangle + (-1)^{I-K}|IM-K\rangle|\bar{\phi}\rangle\right), \tag{9}$$

where $|IMK\rangle$ denotes the Wigner D-function $\sqrt{\frac{2I+1}{8\pi^2}}D^I_{MK}$, which describes the rotational motion of the nucleus by quantum numbers $I$, $M$, and $K$; $|\phi\rangle$ is an intrinsic wave function that describes the motion of valence nucleons; and the coefficients $C_{K\phi}$ are the amplitudes of the basis states. $I$ is the total angular momentum quantum number of the nucleus, and the projections of the total angular momentum vector $\boldsymbol{I}$ on the $z$ axis in the laboratory frame and the $z$ axis (3-axis) in the body-fixed frame are denoted by $M$ and $K$, respectively.

### C. Angular momentum geometry analysis

The reduced transition probabilities $B(M1)$ and $B(E2)$, as fingerprints of nuclear chirality, can be calculated from the total wave function of the PRM [4].

The probability distribution for the projection $K$ of the total angular momentum vector $\boldsymbol{I}$ on the three principle axes ($K$-plot) is [5, 12]

$$P_K = \sum_{\phi} |C_{K\phi}|^2. \tag{10}$$

The profile for the orientation of the angular momentum in the intrinsic reference frame (azimuthal plot) can also be calculated from the total wave function [12, 32, 34, 65],

$$\mathscr{P}(\theta,\varphi) = 2\pi \sum_{\phi'} \left| \sum_{K,\phi} c_{K,\phi} \sqrt{\frac{2I+1}{16\pi^2}} \left[D^I_{IK}(\psi,\theta,\pi-\varphi)\delta_{\phi',\phi} + (-1)^{I-K} D^I_{I-K}(\psi,\theta,\pi-\varphi)\delta_{\phi',-\phi}\right] \right|^2, \tag{11}$$

with the expectation value $M = I$ in the intrinsic frame.

## III. NUMERICAL DETAILS

As mentioned in Sec. I, the one-particle-one-hole configuration $\pi f^{-1}_{7/2} \otimes \nu g^1_{9/2}$ is adopted in the PRM calculations. In Ref. [56], the configuration $\pi f^{-1}_{7/2} \otimes \nu g^1_{9/2}$ favorable for nuclear chirality appears at the quadrupole deformation parameter $\beta \approx 0.25$. According to the results for $^{60}$Ni presented in Refs. [12, 66, 67], the range of the moment of inertia $\mathscr{J}$ can be estimated using the relationship between energy and moment of inertia given by the formula $E_I = I(I+1)\hbar^2/2\mathscr{J}$. The estimated range for $\mathscr{J}$ is from 5 to 13 $\hbar^2$/MeV. Additionally, the energy difference $\Delta E$ is not sensitive to $\beta$ and $\mathscr{J}$ according to PRM calculations. Therefore, $\beta$ is initially set to 0.25 and $\mathscr{J}$ to the approximate middle value of 10 $\hbar^2$/MeV. The triaxial deformation parameter $\gamma$ is then varied to identify its optimal value to ultimately derive the optimal set of input parameter values about $\gamma$, $\beta$, and $\mathscr{J}$. In the calculation of the electromagnetic transitions, the empirical intrinsic quadrupole moment $Q_0 = (3/\sqrt{5\pi})R_0^2 Z\beta$ is set at 1.28 $e$b. The gyromagnetic ratios for the rotor $g_R = Z/A = 0.48$, $g_p = 1 + (g_s - 1)/(2l+1) = 1.336$, and $g_n = g_s/(2l+1) = -0.255$ (where $g_s$ is $0.6g_s^{\rm free}$ [59]) have been adopted based on the $A \approx 60$ mass region.

## IV. RESULTS AND DISCUSSIONS

### A. Influence of triaxial deformation parameter

The energy spectra of the two lowest bands $A$ and $B$ are presented as red and blue lines in Fig. 1, respectively, and calculated using the PRM when the triaxial deformation parameter $\gamma$ varies from 15° to 45°. When the chiral doublet bands appear with the smallest difference in energy, the best known condition is the maximum triaxiality $\gamma = 30°$ when the configuration is symmetrical [2]. However, in Fig. 1, the best condition deviates the maximum triaxiality to $\gamma \sim 34°$ owing to the asymmetrical configuration $\pi f^{-1}_{7/2} \otimes \nu g^1_{9/2}$. For $\gamma = 30°$, the energies of bands $A$ and $B$ similarly increase from $I = 9$ to $15\hbar$, and the energy difference between the two bands $A$ and $B$ exhibits a trend that initially decreases from $I = 9$ to $10\hbar$ and then increases up to $I = 15\hbar$. The minimum energy splitting $\Delta E$ is small (171 keV) but not the smallest. When $\gamma$ increases from 15° to 45°, $\Delta E$ initially decreases and then increases, with the smallest value (64 keV) for $\gamma = 34°$ concerning the best degeneracy. The energy of bands $A$ and $B$ are nearly identical at $I = 9$ and $10\hbar$, corresponding to the ideal chirality. As $\gamma$ deviates further from 34°, the difference between the doublet bands in energy becomes more pronounced, which means that the degeneracy is gradually removed. Hence, the best possible triaxial deformation condition in this research about chiral doublets is $\gamma = 34°$.

The calculated intraband reduced magnetic dipole transition probabilities $B(M1)$ of bands $A$ and $B$ with different triaxiality parameters $\gamma$ are shown in Fig. 2. The central panel of Fig. 2 shows the calculated $B(M1)$ of doublet bands with $\gamma = 30°$. For $I \leqslant 11\hbar$, the intraband $B(M1)$ decreases gradually with spin. For $I > 11\hbar$, a strong odd-even staggering of $B(M1)$ can be observed

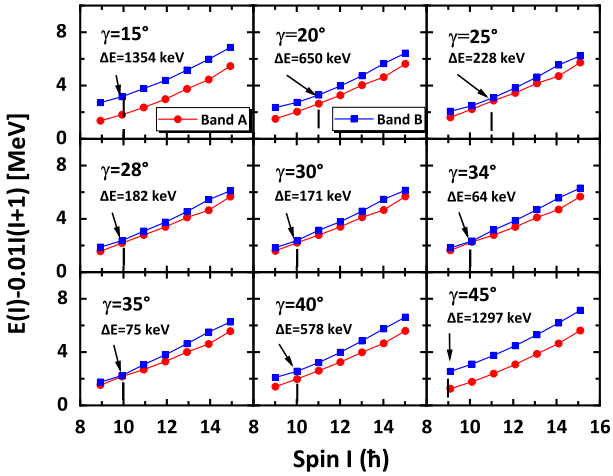


**Fig. 1.** (color online) Energy spectra of the yrast (labeled as band $A$) and yrare (labeled as band $B$) bands calculated using the PRM at different $\gamma$ deformations for the $\pi f_{7/2}^{-1}\otimes\nu g_{9/2}^{1}$ configuration. A rigid rotor reference has been subtracted from the energies. The minimum energy splitting is marked as $\Delta E$ in each panel.

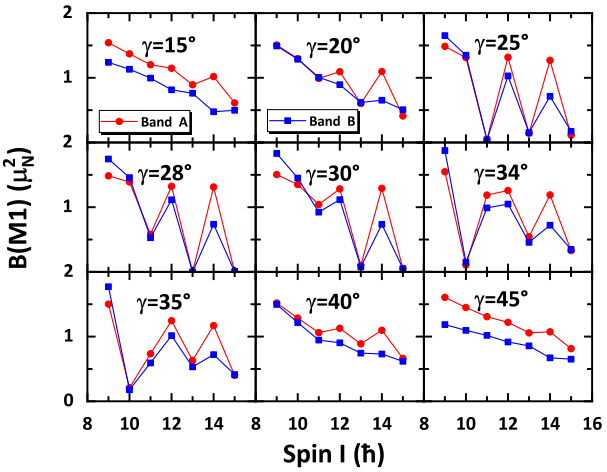


**Fig. 2.** (color online) Same as Fig. 1 but for the intraband $B(M1)$ values.

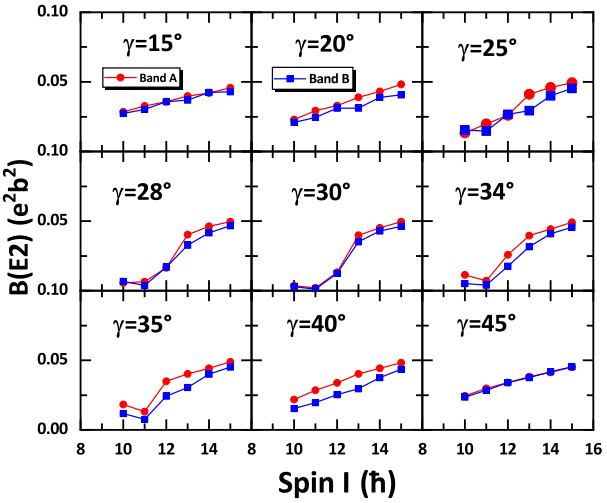


**Fig. 3.** (color online) Same as Fig. 1 but for the intraband $B(E2)$ values.

clearly with the intraband $B(M1)$ transitions enhanced from spin odd to even and forbidden from spin even to odd, implying static chirality [68]. The staggering for band $B$ is slightly weaker than that for band $A$ with a similar tendency. The $B(M1)$ staggering coincides with the odd-even staggering of intraband $B(M1)/B(E2)$ ratios for the ideal chiral doublets [69]. However, as $\gamma$ deviates from the best triaxial deformation 30°, shown in other panels of Fig. 2, the pronounced $B(M1)$ staggering at $\gamma = 30°$ becomes increasingly weaker and gradually moves to the high spin region. At $\gamma = 15°$ and 45°, the $B(M1)$ staggering completely disappears in band $B$ and only a very weak staggering still exists in band $A$ from $I = 13$ to $16\hbar$. This suggests that the $B(M1)$ staggering will gradually disappear for $I > 11\hbar$ when $\gamma$ deviates from 30°, indicating a transition from static chirality to chiral vibration [68]. Thus, a $\gamma$ value of 34° near 30° is reasonable.

The calculated intraband reduced electric quadrupole transition probabilities $B(E2)$ as functions of spin of bands $A$ and $B$ with different triaxiality parameters $\gamma$ are plotted in Fig. 3. The central panel of Fig. 3 shows the calculated $B(E2)$ of doublet bands with $\gamma = 30°$. For $I \leqslant 11\hbar$, the intraband $E2$ transitions are forbidden. For $I > 11\hbar$, the intraband $B(E2)$ increases with spin. We find that the intraband $B(E2)$ of the two bands are nearly identical, as excepted in ideal chiral doublet bands [70]. The other panels of Fig. 3 show the calculated $B(E2)$ of the two bands with $\gamma$ deviating by 30°. The forbidden $E2$ transitions with $I \leqslant 11\hbar$ are allowed gradually. For $I > 11\hbar$, the intraband $B(E2)$ values are not sensitive to the triaxiality parameter $\gamma$. Moreover, $B(E2)$ values between the partner bands are very similar as $\gamma$ changes from 15° to 45°.

Summarizing the above discussions, the parameters for the ideal chirality with the configuration $\pi f_{7/2}^{-1}\otimes\nu g_{9/2}^{1}$ in the $A \approx 60$ mass region are $\beta = 0.25$, $\gamma = 34°$, and $\mathcal{J} = 10\,\hbar^2/\mathrm{MeV}$.

### B. Influence of proton-neutron residual interaction

In the following, we investigate the effects on the chiral doublet bands caused by the residual proton-neutron interaction ($V_{pn}$). The strength parameters $u_0$ and $u_1$ in the residual interaction, which has a standard delta function form (7), are introduced and the above ideal parameters are adopted. The other parameters remain unchanged.

The energy splitting $\Delta E(I)$ from PRM calculations with and without $V_{pn}$ and for different values of spin-spin strength parameter $u_1$ and relative strength ratio $u_0 : u_1$

are shown in Fig. 4. For $u_1 = -0.2$ MeV and $u_0 : u_1 = 3 : 1$, the splitting $\Delta E$ is nearly identical to the result without $V_{pn}$. When $u_1$ remains constant, $\Delta E$ with $V_{pn}$ tends to increase in the high spin region as $u_0 : u_1$ increases. Moreover, when the absolute value of $u_1$ increases, the growth trend of $\Delta E$ becomes pronounced. The two $\Delta E$ values with and without $V_{pn}$ are more different, particularly in the high spin region. This indicates that the energy splitting between the doublet bands is significantly influenced by the presence of $V_{pn}$, which is not conducive to the appearance of chirality. Therefore, $V_{pn}$ has a negative impact on the nuclear chirality.

As a fingerprint of nuclear chirality, the energy staggering parameter $S(I) = [E(I) - E(I-1)]/2I$ should have a smooth dependence with spin $I$ in the chiral region because the particle and hole orbital angular momenta are both approximately perpendicular to the core rotation [69]. In Fig. 5 the results of quantity $S(I)$ are illustrated as functions of spin. In the absence of $V_{pn}$, the $S(I)$ of doublet bands have small odd-even staggering amplitudes corresponding to the above property smoothly dependent on spin. Additionally, both bands have the same phase, with band $A$ in the 11 to 13$\hbar$ spin region and band $B$ in the 12 to 14$\hbar$ spin region. In contrast, $S(I)$ values of doublet bands have strong odd-even staggering and opposite phases in the other spin region. Attention is then shifted to the results including the residual interaction. When $u_0 : u_1 = 3 : 1$ and $u_1 = -0.2$ MeV, the $S(I)$ results are nearly identical to those without $V_{pn}$. However, the $S(I)$ values in bands $A$ and $B$ have two apparent changes when the absolute value of $u_1$ and $u_0 : u_1$ are enhanced. The first one is that the $S(I)$ of the two bands have opposite phases in the entire spin region. The other one is that the odd-even staggering becomes large and changes phases as spin increases compared with those results without $V_{pn}$. The inverted phase observed at high spins, along with the opposing phases of the double bands, results from the signature inversion induced by the introduction of $V_{pn}$ under the condition of triaxiality [57]. Therefore, considering $V_{pn}$, it is reasonable for nuclear chirality to have small values for $|u_1|$ and $u_0 : u_1$, which corresponds to the spin smooth dependence of $S(I)$.

The calculated values of $B(E2)$ and $B(M1)$ in the doublet bands with and without $V_{pn}$ are presented in Figs. 6 and 7, respectively. Fig. 6 shows that $V_{pn}$ does not significantly influence the $B(E2)$ values of bands $A$ and $B$, indicating a negligible effect of $V_{pn}$ on the collective rotation. As shown in Fig. 7, when $u_1$ is $-0.2$ MeV and $u_0 : u_1$ is $3 : 1$, the $B(M1)$ values of the two bands are nearly identical to that in the middle-right panel of Fig. 2, whether $V_{pn}$ is considered or not. When the absolute value of $u_1$ and $u_0 : u_1$ increase, the $B(M1)$ odd-even staggering amplitudes are only slightly enhanced at high spins, which suggests the weak effect of $V_{pn}$ on $B(M1)$. Generally, $V_{pn}$ exhibits no discernible impact on the electromagnetic transition probabilities used as fingerprints for the chiral doublet bands in this work.

### C. Evolution of chiral modes

To further understand the evolution of the chirality with spin $I$, the $K$ distribution of total angular momentum $K_l$, $K_i$, and $K_s$ on the three principle axes for bands $A$ and $B$ in PRM with and without $V_{pn}$ are displayed in Fig. 8 for $I = 9,\ 10,\ 11\hbar$, corresponding to the spin region for the good energy degeneracy in Fig. 4. As shown in the results without $V_{pn}$, for $I = 9\hbar$, the $K$ distributions for bands $A$ and $B$ are somewhat different. The peaks of $K_i$ distributions are located at $K_i = 1\hbar$ for band $A$ (symmetric zero-

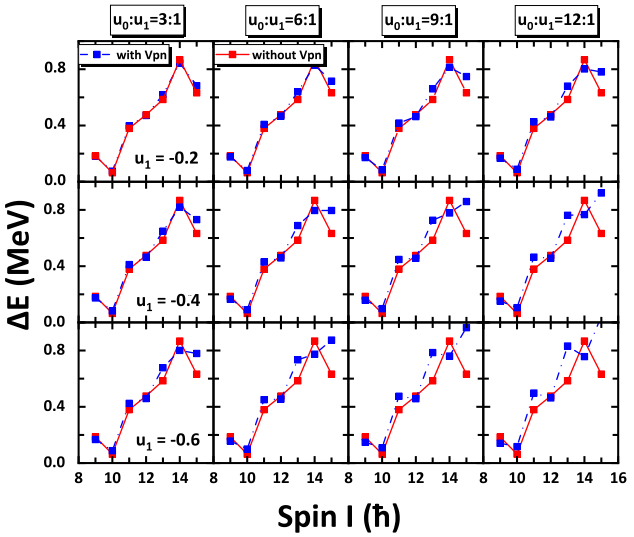


**Fig. 4.** (color online) Energy difference $\Delta E(I)$ between the doublet bands calculated using the PRM without and with $V_{pn}$ at different strength parameters $u_1 = -0.2,\ -0.4,\ -0.6$ MeV and $u_0 : u_1 = 3 : 1,\ 6 : 1,\ 9 : 1,\ 12 : 1$.

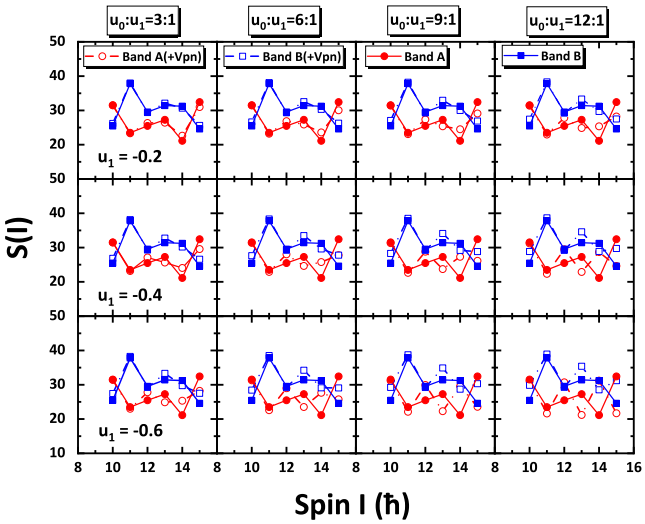


**Fig. 5.** (color online) Same as Fig. 4 but for the staggering parameter $S(I) = [E(I) - E(I-1)]/2I$.

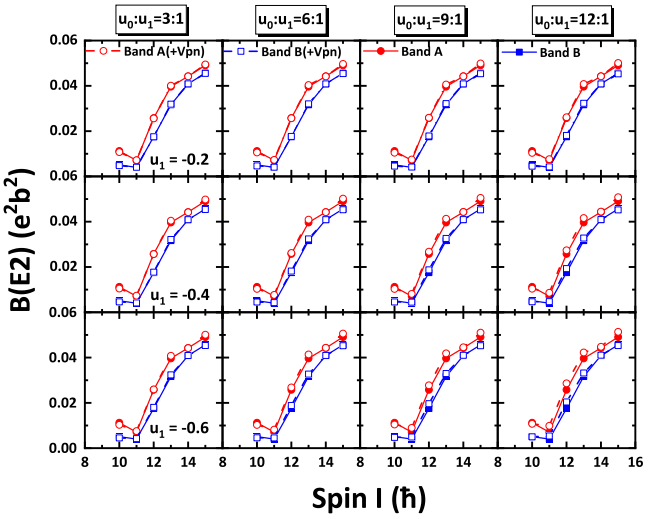


**Fig. 6.** (color online) Same as Fig. 4 but for the intraband $B(E2)$ values.

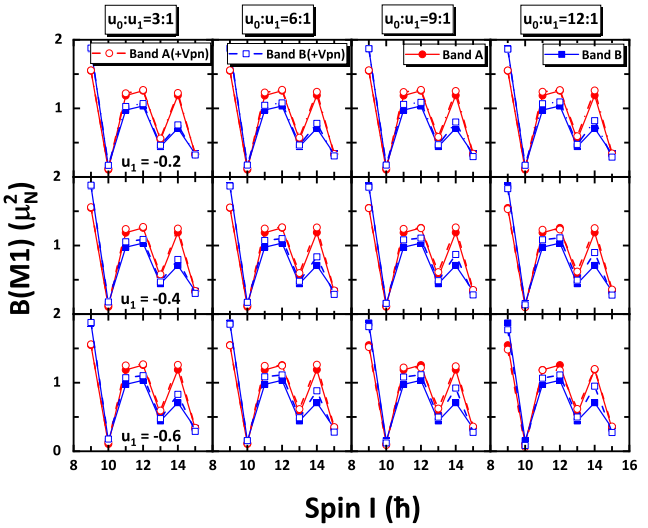


**Fig. 7.** (color online) Same as Fig. 4 but for the intraband $B(M1)$ values.

phonon state) and at $K_i = 6\hbar$ for band $B$ (antisymmetric one-phonon state) [5, 68]. The peaks of $K_l$ and $K_s$ distributions are both located at $6\hbar$ for band $A$ and at $4\hbar$ and $8\hbar$, respectively, for band $B$. The $K$ distributions suggest a typically chiral vibration with an oscillation of the collective core angular momentum $R$ through the $sl$-plane. For $I = 10$ and $11\hbar$, the $K_i$ distributions between bands $A$ and $B$ are similar. The $K_l$ distribution of band $A$ has a bump at lower $K_l$ values, whereas it has a similar bump at higher $K_l$ values for band $B$. These indicate that bands $A$ and $B$ have the characteristics of static chirality.

Reexamining the middle-right panel of Fig. 2, we find that the pronounced $B(M1)$ staggering for $I = 10$, $11\hbar$ corresponds with the above static chirality spin region of $K$ distributions. Now, considering $V_{pn}$, Fig. 8 shows that the results with and without $V_{pn}$ are similar, suggesting

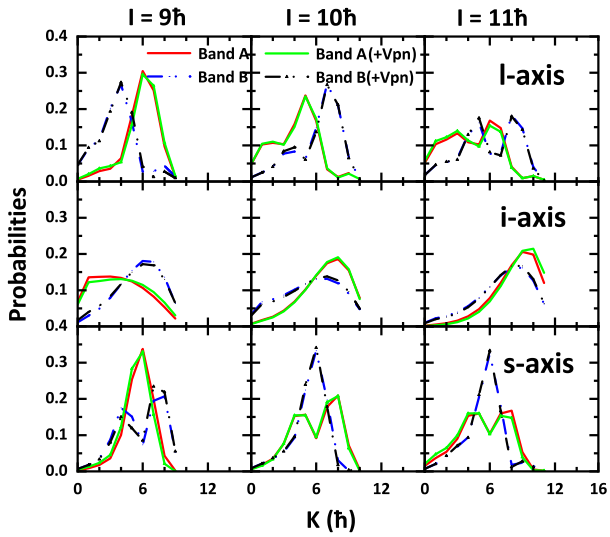


**Fig. 8.** (color online) Probability distributions for projections $K$ of total angular momentum $\boldsymbol{I}$ on the long ($l$), intermediate ($i$), and short ($s$) axes for bands $A$ and $B$ in the PRM with and without $V_{pn}$ for maximum strength parameters $u_0 = -7.2$ MeV, $u_1 = -0.6$ MeV at $I = 9$, 10, $11\hbar$.

the slight effect of $V_{pn}$ on characteristics of chirality with $K$ distributions.

To investigate the angular momentum geometry of the nuclear system in detail, the azimuthal plots [12, 32, 34, 65] (also called spin coherent state maps [71]), *i.e.*, profiles $\mathscr{P}(\theta,\varphi)$ of the doublet bands on the $(\theta,\varphi)$ plane, calculated using the PRM with $V_{pn}$ with maximum strength parameters of $u_0 = -7.2$ MeV and $u_1 = -0.6$ MeV at $I = 8$-$12\hbar$, are shown in Fig. 9. Here, $\theta$ is the angle between the total angular momentum $\boldsymbol{I}$ and the $l$ axis, and $\varphi$ is the angle between the projection of $\boldsymbol{I}$ onto the $si$ plane and the $s$-axis. Note that the azimuthal plots are symmetric with respect to $\varphi = 0°$ for the sake of the $D_2$ symmetry.

For $I = 8$ and $9\hbar$, the angular momentum for band $A$ mainly orientates at $(\theta \sim 45°, \varphi = 0°)$, corresponding to a planar rotation within the $sl$ plane. The angular momentum for band $B$ orientates equally at $(\theta \sim 45°, \varphi \sim \pm 60°)$, and the maximum of $\mathscr{P}(\theta,\varphi)$ is evidently smaller than that of band $A$, understood as a realization of chiral vibration along the $\theta$ direction (*i.e.*, with respect to the $sl$ plane). This is consistent with the different $K$ distributions between the doublet bands at $I = 9\hbar$ in Fig. 8 in that the $i$ component of the rotator angular momentum for band $B$ is larger than that for band $A$.

For $I = 10\hbar$, the angular momentum orientates equally at two aplanar directions, *i.e.*, $(\theta \sim 55°, \varphi \sim \pm 70°)$ for band $A$, while $(\theta \sim 55°, \varphi \sim \pm 30°)$ for band $B$. These characteristics demonstrate the occurrence of static chirality that accounts for the similar $K$ distributions between the doublet bands in Fig. 8 and hence yield the lowest $\Delta E$ at $10\hbar$, as shown in the bottom-right panel of Fig. 4.

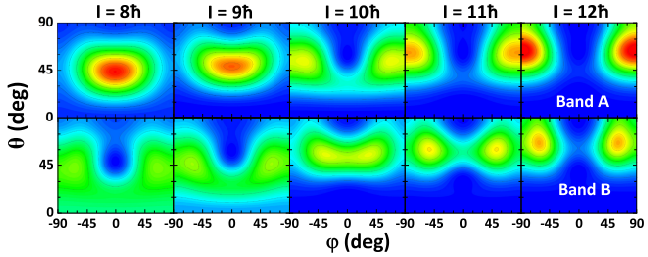


**Fig. 9.** (color online) Azimuthal plots (*i.e.*, profiles for the orientation of the angular momentum) on $(\theta,\varphi)$ plane calculated using the PRM with $V_{pn}$ with maximum strength parameters $u_0 = -7.2$ MeV, $u_1 = -0.6$ MeV at $I = 8$-$12\hbar$, respectively.

For $I = 11\hbar$, the angular momentum orientates equally at $(\theta \sim 60^\circ, \varphi \sim \pm 85^\circ)$ for band $A$ and at $(\theta \sim 60^\circ, \varphi \sim \pm 50^\circ)$ for band $B$. At this critical spin, the rotational mode of band $A$ changes from an aplanar rotation back to a nearly planar rotation within the $li$ plane, which weakens the static chirality.

For $I = 12\hbar$, the static chirality disappears. The angular momentum for band $A$ orientates at $(\theta \sim 65^\circ, \varphi \sim \pm 90^\circ)$, namely in the $li$ plane and close to the $i$ axis. The angular momentum for band $B$ orientates equally at $(\theta \sim 65^\circ, \varphi \sim \pm 60^\circ)$, corresponding to an aplanar rotation. At this spin, a new type of chiral vibration appears within the $li$ plane [12], which is consistent with the vanishing $B(M1)$ staggering from $I = 11$ to $12\hbar$, as shown in the bottom-right panel of Fig. 7.

Figs. 8 and 9 illustrate the transition of chirality from chiral vibration to static chirality and then to another type of chiral vibration as spin increases from 8 to $12\hbar$.

## V. SUMMARY

For Co isopotes with the configuration $\pi f_{7/2}^{-1} \otimes \nu g_{9/2}^{1}$ in the $A \approx 60$ mass region, optimal parameter values for the ideal chiral bands have been determined through assessments of chiral features, *i.e.*, the energy degeneracy of doublets, the staggering of $B(M1)$, and the similarity of $B(E2)$. These parameters are determined to be $\gamma = 34^\circ$, $\beta = 0.25$, and $\mathscr{J} = 10\,\hbar^2/\text{MeV}$ according to the PRM calculations.

With the inclusion of the residual proton-neutron interaction $V_{pn}$ in the PRM adopting the above optimal parameters, the chirality of the nuclear system is discussed in detail. The electromagnetic transition probabilities are slightly affected by the presence of $V_{pn}$. Nevertheless, the energy splitting $\Delta E(I)$ and energy staggering parameter $S(I)$ demonstrate that lower values of the strength parameter $|u_0|$ and relative strength ratio $u_0 : u_1$ are more favorable for the existence of chiral doublet bands. In addition, the evolution of the chirality is suggested based on the $K$-plots and the azimuthal plots $\mathscr{P}(\theta,\varphi)$, namely, a chiral vibration appears at $I = 8\hbar$, changes to static chirality at $I = 10\hbar$, and finally evolves to another type of chiral vibration at $I = 12\hbar$.

The present results identify optimal conditions for chiral doublet bands in the $A \approx 60$ mass region using the PRM and explore the residual proton-neutron interaction $V_{pn}$ as an effect factor. We hope that the PRM containing $V_{pn}$ can be applied in future studies of nuclear chiral features (particularly the energy staggering $S(I)$) in different mass regions. Furthermore, note that in the current study, the core is a rigid rotor. The effect of residual proton-neutron interaction $V_{pn}$ in a soft core, *e.g.*, using the IBFFM [25–27, 72], would be interesting to consider. Additionally, an experimental opportunity is presented for the observation of chiral doublet bands in the $A \approx 60$ mass region.

## References


[1] S. Frauendorf and J. Meng, Nucl. Phys. A **617**, 131 (1997)
[2] J. Peng, J. Meng, and S. Q. Zhang, Phys. Rev. C **68**, 044324 (2003)
[3] T. Koike, K. Starosta, and I. Hamamoto, Phys. Rev. Lett. **93**, 172502 (2004)
[4] S. Q. Zhang, B. Qi, S. Y. Wang *et al.*, Phys. Rev. C **75**, 044307 (2007)
[5] B. Qi, S. Q. Zhang, J. Meng *et al.*, Phys. Lett. B **675**, 175 (2009)
[6] Q. B. Chen, J. M. Yao, S. Q. Zhang *et al.*, Phys. Rev. C **82**, 067302 (2010)
[7] E. A. Lawrie and O. Shirinda, Phys. Lett. B **689**, 66 (2010)
[8] I. Hamamoto, Phys. Rev. C **88**, 024327 (2013)
[9] H. Jia, B. Qi, S. Y. Wang *et al.*, Chin. Phys. C **40**, 124103 (2016)
[10] Q. B. Chen, B. F. Lv, C. M. Petrache *et al.*, Phys. Lett. B **782**, 744 (2018)
[11] Y. Y. Wang, S. Q. Zhang, P. W. Zhao *et al.*, Phys. Lett. B **792**, 454 (2019)
[12] J. Peng and Q. B. Chen, Phys. Lett. B **793**, 303 (2019)
[13] Y. P. Wang, Y. Y. Wang, and J. Meng, Phys. Rev. C **102**, 024313 (2020)
[14] Q. B. Chen, N. Kaiser, U.-G. Meißner *et al.*, Phys. Lett. B **807**, 135568 (2020)
[15] J. Peng and Q. B. Chen, Phys. Lett. B **806**, 135489 (2020)
[16] Y. Zhang, B. Qi, and S. Q. Zhang, Sci. China-Phys. Mech. Astron. **64**, 122011 (2021)
[17] A. A. Raduta, A. H. Raduta, and C. M. Petrache, J. Phys. G: Nucl. Part. Phys. **43**, 095107 (2016)
[18] R. Budaca, Phys. Rev. C **98**, 014303 (2018)
[19] R. Budaca, Phys. Lett. B **797**, 134853 (2019)
[20] V. I. Dimitrov, S. Frauendorf, and F. Dönau, Phys. Rev. Lett. **84**, 5732 (2000)
[21] P. Olbratowski, J. Dobaczewski, J. Dudek *et al.*, Phys. Rev. Lett. **93**, 052501 (2004)
[22] P. W. Zhao, S. Q. Zhang, and J. Meng, Phys. Rev. C **92**, 034319 (2015)
[23] P. W. Zhao, Phys. Lett. B **773**, 1 (2017)
[24] Z. X. Ren, P. W. Zhao, and J. Meng, Phys. Rev. C **105**, L011301 (2022)

[25] D. Tonev, G. de Angelis, P. Petkov *et al.*, Phys. Rev. Lett. **96**, 052501 (2006)
[26] D. Tonev, G. d. Angelis, S. Brant *et al.*, Phys. Rev. C **76**, 044313 (2007)
[27] S. Brant, D. Tonev, G. De Angelis *et al.*, Phys. Rev. C **78**, 034301 (2008)
[28] S. Mukhopadhyay, D. Almehed, U. Garg *et al.*, Phys. Rev. Lett. **99**, 172501 (2007)
[29] D. Almehed, F. Dönau, and S. Frauendorf, Phys. Rev. C **83**, 054308 (2011)
[30] Q. B. Chen, S. Q. Zhang, P. W. Zhao *et al.*, Phys. Rev. C **87**, 024314 (2013)
[31] Q. B. Chen, S. Q. Zhang, P. W. Zhao *et al.*, Phys. Rev. C **94**, 044301 (2016)
[32] Q. B. Chen and J. Meng, Phys. Rev. C **98**, 031303 (2018)
[33] G. H. Bhat, R. N. Ali, J. A. Sheikh *et al.*, Nucl. Phys. A **922**, 150 (2014)
[34] F. Q. Chen, Q. B. Chen, Y. A. Luo *et al.*, Phys. Rev. C **96**, 051303 (2017)
[35] F. Q. Chen, J. Meng, and S. Q. Zhang, Phys. Lett. B **785**, 211 (2018)
[36] M. Shimada, Y. Fujioka, S. Tagami *et al.*, Phys. Rev. C **97**, 024319 (2018)
[37] Y. K. Wang, F. Q. Chen, P. W. Zhao *et al.*, Phys. Rev. C **99**, 054303 (2019)
[38] Y. K. Wang, P. W. Zhao, and J. Meng, Phys. Lett. B **848**, 138346 (2024)
[39] B. Li, P. W. Zhao, and J. Meng, Phys. Lett. B **856**, 138877 (2024)
[40] S. Frauendorf, Rev. Mod. Phys. **73**, 463 (2001)
[41] J. Meng, B. Qi, S. Q. Zhang *et al.*, Mod. Phys. Lett. A **23**, 2560 (2008)
[42] J. Meng and S. Q. Zhang, J. Phys. G: Nucl. Part. Phys. **37**, 064025 (2010)
[43] R. A. Bark, E. O. Lieder, R. M. Lieder *et al.*, Int. J. Mod. Phys. E **23**, 1461001 (2014)
[44] J. Meng and P. W. Zhao, Phys. Scr. **91**, 053008 (2016)
[45] A. A. Raduta, Prog. Part. Nucl. Phys. **90**, 241 (2016)
[46] K. Starosta and T. Koike, Phys. Scr. **92**, 093002 (2017)
[47] B. W. Xiong and Y. Y. Wang, Atom. Data Nucl. Data Tables **125**, 193 (2019)
[48] Q. B. Chen and J. Meng, Nuclear Physics News **30**, 11 (2020)
[49] S. Y. Wang, Chin. Phys. C **44**, 112001 (2020)
[50] S. Y. Wang, C. Liu, B. Qi *et al.*, Front. Phys. **18**, 64601 (2023)
[51] R. Budaca, Front. Phys. **19**, 24301 (2024)
[52] R. A. Bark, E. A. Lawrie, C. Liu *et al.*, Front. Phys. **19**, 24302 (2024)
[53] R. V. Jolos, E. A. Kolganova, and D. R. Khamitova, Front. Phys. **19**, 24303 (2024)
[54] E. Grodner, M. Kowalczyk, J. Srebrny *et al.*, Front. Phys. **19**, 64601 (2024)
[55] C. M. Petrache, ed., *Chirality and wobbling in atomic nuclei* (CRC Press, Boca Raton, 2024)
[56] J. Peng and Q. B. Chen, Phys. Rev. C **98**, 024320 (2018)
[57] E. A. Lawrie, P. A. Vymers, J. J. Lawrie *et al.*, Phys. Rev. C **78**, 021305 (2008)
[58] A. Bohr and B. R. Mottelson, *Nuclear Structure*, Vol. 2 (Benjamin, 1975) p. 199.
[59] P. Ring and P. Schuck, *The nuclear many-body problem* (Springer-Verlag, 1981) p. 107.
[60] H. Zhang and Q. B. Chen, Chin. Phys. C **40**, 024102 (2016)
[61] J. Meyer-Ter-Vehn, Nucl. Phys. A **249**, 111 (1975)
[62] S. Y. Wang, B. Qi, and S. Q. Zhang, Chin. Phys. Lett. **26**, 052102 (2009)
[63] J. P. Boisson, R. Piepenbring, and W. Ogle, Phys. Rep. **26**, 99 (1976)
[64] N. Tajima, Nucl. Phys. A **572**, 365 (1994)
[65] E. Streck, Q. B. Chen, N. Kaiser *et al.*, Phys. Rev. C **98**, 044314 (2018)
[66] M. A. J. Mariscotti, G. Scharff-GoldHaber, and B. Buck, Phys. Rev. **178**, 1864 (1969)
[67] D. A. Torres, F. Cristancho, L. L. Andersson *et al.*, Phys. Rev. C **78**, 054318 (2008)
[68] B. Qi, S. Q. Zhang, S. Y. Wang *et al.*, Phys. Rev. C **79**, 041302 (2009)
[69] C. Vaman, D. B. Fossan, T. Koike *et al.*, Phys. Rev. Lett. **92**, 032501 (2004)
[70] C. M. Petrache, G. B. Hagemann, I. Hamamoto *et al.*, Phys. Rev. Lett. **96**, 112502 (2006)
[71] Q. B. Chen and S. Frauendorf, Eur. Phys. J. A **58**, 75 (2022)
[72] N. Yoshida, H. Sagawa, and T. Otsuka, Nucl. Phys. A **567**, 17 (1994)